

# Secular dynamics of multiplanet systems: implications for the formation of hot and warm Jupiters via high-eccentricity migration

Adrian S. Hamers<sup>1</sup>\*, Fabio Antonini<sup>2</sup>, Yoram Lithwick<sup>2</sup>, Hagai B. Perets<sup>3</sup> and Simon F. Portegies Zwart<sup>1</sup>

<sup>1</sup>Leiden Observatory, Leiden University, PO Box 9513, NL-2300 RA Leiden, The Netherlands

<sup>2</sup>Center for Interdisciplinary Exploration and Research in Astrophysics (CIERA), and Department of Physics and Astronomy, Northwestern University, 2145 Sheridan Road, Evanston, IL 60208, USA

<sup>3</sup>Technion - Israel Institute of Technology, Haifa 32000, Israel

November 27, 2018

## ABSTRACT

Hot Jupiters (HJs) are Jupiter-like planets that reside very closely to their host star, within  $\sim 0.1$  AU. Their formation is not well understood. It is generally believed that they cannot have formed *in situ*, implying that some form of migration must have occurred after their initial formation. We study the production of HJs through secular evolution in multiplanet systems with three to five planets. In this variant of high- $e$  migration, the eccentricity of the orbit of the innermost planet is excited on secular time-scales, triggering orbital migration due to tidal dissipation. We use a secular dynamics code and carry out a population synthesis study. We find that HJs are only produced if the viscous time-scale is short ( $\approx 0.014$  yr). In contrast, in up to  $\approx 0.3$  of systems, the innermost planet is tidally disrupted. The orbital period distribution is peaked around 5 d, consistent with observations. The median HJ mass is  $1 M_J$  with a maximum of  $\approx 2 M_J$ , similar to observed HJs. Approximately 0.1 of the HJs have retrograde orbits with respect to the stellar spin. We do not find any warm Jupiters in our simulations, i.e. planets with semimajor axes between 0.1 and 1 AU.

**Key words:** planets and satellites: dynamical evolution and stability – planet-star interactions – gravitation

## 1 INTRODUCTION

In the past decades, radial velocity and transit methods have revealed a population of gas giant planets of order Jupiter mass around solar-type stars with orbital periods downward of 10 d, i.e. hot Jupiters (HJs). The current consensus is that HJs could not have formed *in situ* in the protoplanetary disc phase because of an insufficient amount of disc material and/or too high temperatures at these close regions to the host star (e.g. Lin et al. 1996; however, recently it has been suggested that *in situ* formation might be possible through core accretion, Lee et al. 2014; Batygin et al. 2015). If HJs were formed at larger separations, i.e. beyond the snow line of one to a few AU, then this implies that they must have experienced strong inwards migration after their formation, by two orders of magnitude in separation. Two main migration scenarios have been proposed: (1) migration induced by orbital energy dis-

sipation due to gas drag in the protoplanetary disc phase (e.g. Goldreich & Tremaine 1980; Lin & Papaloizou 1986; Bodenheimer et al. 2000; Tanaka et al. 2002), and (2) migration induced by tidal dissipation in the HJ, requiring high orbital eccentricity (commonly known as ‘high- $e$ ’ migration).

For high- $e$  migration, various subscenarios have been proposed to drive the high eccentricities needed to produce the observed short orbital periods through tidal dissipation. They include (i) eccentricity excitation because of close encounters between planets (Rasio & Ford 1996; Chatterjee et al. 2008; Ford & Rasio 2008; Jurić & Tremaine 2008), (ii) excitation of the eccentricity because of secular Lidov-Kozai (LK) oscillations (Lidov 1962; Kozai 1962) induced by a distant binary companion star or an additional (massive) planet on an inclined orbit (Wu & Murray 2003; Fabrycky & Tremaine 2007; Naoz et al. 2012; Petrovich 2015a; Anderson et al. 2016; Petrovich & Tremaine 2016), (iii) secular eccentricity excitation induced by a close and coplanar, but eccentric

\* E-mail: hamers@strw.leidenuniv.nl

planetary companion (Petrovich 2015b), and (iv) eccentricity excitation induced by secular chaos in multiplanet systems with at least three planets in mildly inclined and eccentric orbits (Wu & Lithwick 2011; Lithwick & Wu 2011, 2014).

It is currently unclear which of (1) and (2) applies to observed HJs, or if a combination gives rise to HJs. Both scenarios have successes and failures in describing properties of observed HJs. The observed period distribution of HJs peaks around  $\sim 3 - 5$  d, and their eccentricities are close to zero (e.g. Santerne et al. 2016). Most high- $e$  migration scenarios predict that the final orbit of the HJ should indeed be circular and pile up a short period, around  $\sim 3$  d. Disc migration scenarios are more difficult to reconcile with the observed peak in the period distribution (but see Lin et al. 1996). On the other hand, high- $e$  migration through LK cycles in three-body systems (subscenarios ii and iii) require the presence of a stellar binary or compact planetary companion, which have not (yet) been detected around all HJs (e.g. Knutson et al. 2014; Ngo et al. 2015). Moreover, the predicted production rate is too low, and the predicted periods are too short (e.g. Anderson et al. 2016).

Subscenario (iv) involves three or more planets around a single star, i.e.  $N_p \geq 3$  systems (Wu & Lithwick 2011; Lithwick & Wu 2011, 2014). Similarly to three-body systems (i.e. a binary companion or two planets), secular interactions can change the eccentricities of the orbits, in particular the innermost orbit, on long time-scales (i.e. much longer than the orbital periods). For  $N_p = 2$ , high relative inclinations (typically  $\gtrsim 40^\circ$ ) and/or tight and eccentric outer orbits are required to produce high eccentricities. If  $N_p \geq 3$ , then the conditions for producing high eccentricities in the innermost orbit are less stringent. The initial eccentricities and relative inclinations can be much smaller, and the planets need not be very closely spaced. Suborbital effects such as close encounters and mean motion resonances are then typically unimportant, and the long-term evolution is driven mainly by secular interactions. The secular evolution is typically chaotic, giving rise to highly irregular eccentricity oscillations. Over the course of  $\sim 0.1 - 10$  Gyr, high eccentricities can be reached in the inner orbit, potentially leading to HJs. A well known example is the Solar system, in which secular chaos can drive the orbit of Mercury to become unstable (i.e. lead to an ejection of the planet, or a collision of the planet with the Sun) on a time-scale of 5 Gyr, and with a probability of a few per cent (Laskar & Gastineau 2009; Lithwick & Wu 2014).

The less stringent conditions for secular chaos in  $N_p \geq 3$  systems are compatible with current observations of HJs which exclude close-in companions for a subset of HJs, whereas detections of further-away companions (at  $\gtrsim 5 - 10$  AU) are still largely incomplete because of observational limitations. This argument can also be reversed: the production of HJs through secular chaos *requires* further-away companions, therefore such companions are expected to be observed around HJ-hosting stars in the future.

Parameter space studies and/or Monte Carlo studies to quantify observed properties of the HJs in multiplanet systems are still lacking. The long secular time-scales compared to the short orbital periods imply that direct  $N$ -body integrations, such as those carried out by Wu & Lithwick (2011), are computationally very expensive to carry out, especially

considering the large number of parameters. Until recently, secular, orbit-averaged methods valid for high eccentricities and inclinations were limited to  $N_p = 2$  and to systems that are not too compact, as a consequence of the expansion of the Hamiltonian in terms of ratios of binary separations.

In recent work (Hamers & Portegies Zwart 2016), we presented a generalisation of the secular, orbit-averaged method previously applied to hierarchical three-body systems (e.g. Lidov 1962; Kozai 1962; Harrington 1968; Naoz et al. 2013a), to systems composed of nested binary orbits, with an arbitrary number of bodies and an arbitrary hierarchy, and to fifth order in terms of binary separation ratios for binary-binary interactions. In this paper, we apply this method to study the formation of HJs through secular evolution in multiplanet systems with  $N_p = 3$  to  $N_p = 5$  planets. The main practical advantage of this method is that compared to direct  $N$ -body integrations, the evolution can be computed much faster.

Using a combination of population synthesis and grid sampling, we study the dependence of the HJ properties on various parameters, including the efficiency of tidal dissipation, the number of planets, the width of the initial mutual inclination and eccentricity distribution, and the radius of the innermost planet. These parameters, in particular the efficiency of tidal dissipation, are highly uncertain.

The structure of this paper is as follows. In Section 2, we describe the secular method and other assumptions and in Section 3, we verify it by comparing to a (limited) number of direct  $N$ -body integrations. In Section 4, we present the results from the population synthesis study. We discuss our results in Section 5, and conclude in Section 6.

## 2 METHODS AND ASSUMPTIONS

### 2.1 Notations and overview

In Table 1, we give a list of relevant quantities with a description. Where applicable, we give for reference the values of the (initial) parameters that were assumed in the various sections of this paper.

### 2.2 Secular dynamics

To model the long-term gravitational dynamics of the multiplanet system, we used the algorithm SECULARMULTIPLE (Hamers & Portegies Zwart 2016) within the AMUSE framework (Portegies Zwart et al. 2013; Pelupessy et al. 2013). SECULARMULTIPLE applies to self-gravitating systems composed of nested binaries with an arbitrary number of bodies and an arbitrary hierarchy. A multiplanet system is represented as a ‘nested’ hierarchical multiple system of point particles; the star is contained within the ‘innermost’ binary system (i.e. Jacobian coordinates; see e.g. Figure 3 of Hamers & Portegies Zwart 2016). The algorithm is based on an expansion of the Hamiltonian in terms of binary separation ratios, which are assumed to be small. The resulting Hamiltonian is orbit averaged, and the equations of motion, defining a system of ordinary differential equations, are solved numerically in terms of the orbital vectors  $\mathbf{e}_k$  and  $\mathbf{h}_k$  for all binaries  $k$ .

Symbol	Description	Values in section	
		3	4
$N_p$	number of planets	3	3-5
$M_*$	stellar mass	$1 M_\odot$	$1 M_\odot$
$m_i$	mass of planet $i$	$3 \times 10^{-4} M_\odot (i=1)$ $1 \times 10^{-4} M_\odot (i>1)$	0.5-5 $M_J$
$R_*$	stellar radius	$1 R_\odot$	$1 R_\odot$
$R_i$	radius of planet $i$	$1 R_J$	$1-1.5 R_J$
$\eta$	tidal disruption factor (cf. equation 6)	—	2.7
$t_{V,*}$	stellar viscous time-scale	—	5 yr
$t_{V,1}$	planet 1 viscous time-scale	$\approx 4.8$ yr	0.0137, 0.137, 1.37 yr
$k_{AM,*}$	stellar apsidal motion constant	—	0.014
$k_{AM,1}$	planet 1 apsidal motion constant	0.19	0.25
$r_{g,*}$	stellar gyration radius	—	0.08
$r_{g,1}$	planet 1 gyration radius	—	0.25
$P_{s,*}$	stellar spin period	—	10 d
$P_{s,1}$	planet 1 spin period	—	10 hr
$\theta_*$	stellar obliquity (stellar spin-orbit 1 angle)	—	$0^\circ$
$\theta_1$	planet 1 obliquity (planet 1 spin-orbit 1 angle)	—	$0^\circ$
$a_i$	planet $i$ orbital semimajor axis	1 AU ( $i=1$ ) 6 AU ( $i=2$ ) 12-62 AU ( $i=3$ )	1-4 AU ( $i=1$ ) 6-10 AU ( $i=2$ ) 15-30 AU ( $i=3$ ) 35-50 AU ( $i=4$ ) 60-100 AU ( $i=5$ )
$e_i$	planet $i$ orbital eccentricity	$\approx 0.4-0.6$	0-0.8
$i_i$	planet $i$ orbital inclination <sup>1</sup>	—	0- $30^\circ$
$\omega_i$	planet $i$ argument of pericenter	0- $360^\circ$	0- $360^\circ$
$\Omega_i$	planet $i$ longitude of ascending node	0- $360^\circ$	0- $360^\circ$
$\beta$	width of inclination and eccentricity distribution	—	8.2, 14.6, 32.8

**Table 1.** Description of the quantities used. Where applicable, we give the values of the (initial) parameters that are assumed in Sections 3 and 4.

As shown in Hamers & Portegies Zwart (2016), depending on the compactness of the system, high orders are required to accurately describe the orbital evolution. Here, we included terms corresponding to binary-binary interactions (pairwise terms) up and including fifth order in the separation ratios. To third order ('octupole order'), we included the triplet binary terms (corresponding to interactions between three binaries), although these terms are unimportant for multiplanet systems with roughly equal-mass planets (Hamers & Portegies Zwart 2016). For the fourth and fifth orders, terms associated with interactions between more than two binaries were not included; as shown in Hamers & Portegies Zwart (2016), these terms are unimportant compared to the pairwise binary terms.

Relativistic corrections were included by adding the orbit-averaged precession rates of the line of apsides to the orbits, to the first post-Newtonian (PN) order. Terms in the PN potential associated with interactions between binaries (e.g. Naoz et al. 2013b) were neglected (see also Appendix A7 of Hamers & Portegies Zwart 2016).

### 2.3 Tidal evolution

The tidal evolution of the innermost planet and the star was modeled with the equilibrium tide model of Eggleton et al. (1998). This model also includes the effect of precession of the orbit of the innermost planet due to tidal bulges and spin-orbit coupling. The equilibrium tide model is described in terms of the viscous time-scale  $t_V$ , the apsidal motion constant  $k_{AM}$ , the gyration radius  $r_g$  and the initial spin period  $P_s$ , for both the star and the innermost planet. Our assumed values are given in Table 1. Most of the values are adopted from Fabrycky & Tremaine (2007).

We assumed a constant tidal viscous time-scale  $t_V$  for both the star and the innermost planet. Apart from its simplicity, a temporally constant  $t_{V,1}$  for the innermost planet during high- $e$  migration follows from the equations of motion with a number of physically-motivated assumptions (Socrates & Katz 2012). We note that our assumption of a constant  $t_{V,1}$  is in contrast to Wu & Murray (2003); Wu & Lithwick (2011), who assumed a  $t_{V,1}$  depending on the orbital period (Socrates et al. 2012).

### 3 VERIFICATION OF THE SECULAR METHOD WITH $N$ -BODY INTEGRATIONS

As mentioned in Section 1, the secular evolution of multi-planet systems can be chaotic, especially when the number of planets is  $N_p \geq 3$ . In direct  $N$ -body integrations, this implies that changing the initial orbital phases or the accuracy of the integration can lead to a completely different outcome after some time during which the eccentricities have changed by, say, order unity. This implies that it is not very meaningful – on a one-to-one basis – to compare results from direct  $N$ -body integrations to those from SECULARMULTIPLE, in which the orbits are averaged over. Our expectation is that SECULARMULTIPLE produces the correct secular dynamical evolution in a *statistical* sense, i.e. for an ensemble of systems.

In this section, we investigate this expectation by comparing results from SECULARMULTIPLE to those from the direct  $N$ -body code ARCHAIN (Mikkola & Merritt 2008). The latter code uses algorithmic chain regularisation to integrate the equations of motion with high precision. In addition to relativistic corrections, tidal interactions are taken into account with the same model assumed for the secular integrations. For more details regarding the direct  $N$ -body code, we refer to Antonini et al. (2016) and Antonini et al. (in preparation).

#### 3.1 Initial conditions

The ARCHAIN code was used to integrate 100 three-planet systems for  $\approx 120$  Myr (cf. Table 1). The stellar mass was set to  $M_\star = 1 M_\odot$ , and the planetary masses were assumed to be  $m_1 = 3 \times 10^{-4} M_\odot \approx 0.314 M_J$  and  $m_2 = m_3 = 1 \times 10^{-3} M_\odot \approx 1.05 M_J$ . The initial semimajor axes were assumed to be  $a_1 = 1$  AU,  $a_2 = 6$  AU, and  $a_3$  was varied between 12 and 62 AU with increments of 0.5 AU. The eccentricities and inclinations for all orbits were set equal to each other, and values were assumed ranging between  $\approx 0.4$  and 0.6 (with the inclinations measured in radians). The other orbital angles,  $\omega_i$  and  $\Omega_i$ , were sampled from flat distributions between 0 and  $360^\circ$ . The innermost planet was assumed to have a radius  $R_1 = 1 R_J$ , a viscous time-scale  $t_{V,1} \approx 4.8$  yr, and an apsidal motion constant  $k_{AM,1} = 0.19$ . Tidal disruptions were not checked for (in contrast to Section 4).

#### 3.2 Results

With ARCHAIN, a fraction of 0.32 of the systems became HJ systems by 120 Myr, i.e. the final semilatus rectum of the orbit of the innermost planet,  $r_{1,slr,f} \equiv a_{1,f} (1 - e_{1,f}^2)$ , reached  $r_{1,slr,f} < 0.091$  AU, corresponding to the semimajor axis of a 10-d planet in a circular orbit around a Solar-mass star. We use the semilatus rectum to define HJs, because after 120 Myr, some systems were still decaying tidally (i.e.  $a_1$  and  $e_1$  decreasing), while decoupled from the secular oscillations. In the latter case, when tidal evolution dominates, the final result (i.e. after  $\gg 120$  Myr) is a circular orbit with semimajor axis  $a_{1,f} = r_{1,slr,f}$ . The HJ fraction after 120 Myr of evolution obtained with SECULARMULTIPLE is 0.33.

In Fig. 1, we show the distribution of  $r_{1,slr,f}$  after

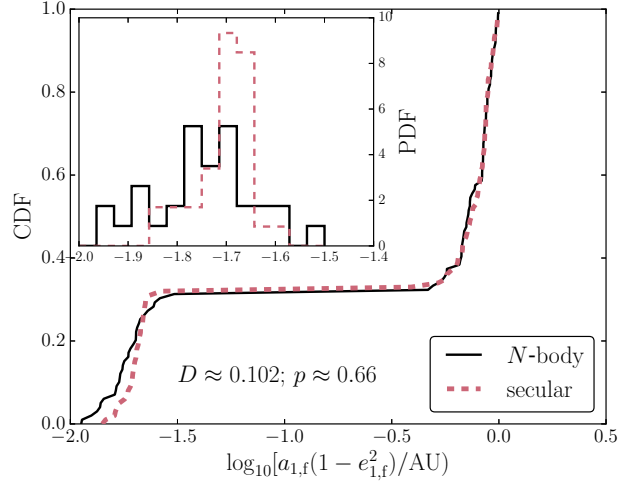


**Figure 1.** The distributions of the innermost planet’s orbit semilatus rectum,  $r_{1,slr,f} \equiv a_{1,f} (1 - e_{1,f}^2)$ , after 120 Myr of evolution according to ARCHAIN (black solid line) and to SECULARMULTIPLE (red dashed line). The  $D$  and  $p$  statistics for the two-sided K-S test between the distributions are indicated in the panel. In the inset, the PDF is shown for  $\log_{10}(r_{1,slr,f}/\text{AU}) < -1.5$ .

120 Myr of evolution in terms of the cumulative density function (CDF) according to ARCHAIN (black solid line) and according to SECULARMULTIPLE (red dashed line). There is a pileup of systems around  $\log_{10}(r_{1,slr,f}/\text{AU}) \approx -1.7$  corresponding to systems in which a HJ was formed. The number of systems subsequently stalls at  $\approx 0.32$  with increasing  $r_{1,slr,f}$ , until at  $\log_{10}(r_{1,slr,f}/\text{AU}) \approx -0.4$ , this number increases again. The latter correspond to non- (or weakly) migrating planets; either their semimajor axes have decreased slightly due to tidal evolution, and/or their eccentricities are excited because of secular evolution.

In terms of  $r_{1,slr,f}$ , there is statistical agreement between ARCHAIN and SECULARMULTIPLE; the two-sided Kolmogorov-Smirnov (K-S; Kolmogorov 1933; Smirnov 1948) test statistics are  $D \approx 0.082$  and  $p \approx 0.881$ . There is a tendency for SECULARMULTIPLE to (slightly) overestimate the smallest semilatus recta, or the smallest orbital periods of the HJs, compared to ARCHAIN. We do not believe that this discrepancy strongly affects our conclusions in the integrations in Section 4.

In Fig. 2, we show another comparison between the two methods in terms of the distributions of the HJ formation times, i.e. the times when  $r_{1,slr,f} \lesssim 0.09$  AU (corresponding to an orbital period of 10 d around a solar-mass star). With both methods, most ( $\approx 0.7$ ) HJs are produced early in the evolution, i.e. within the first 10 Myr. The K-S test yields  $D \approx 0.16$  and  $p \approx 0.763$ , showing that the two distributions are statistically consistent. Nonetheless, the formation times in SECULARMULTIPLE after 10 Myr tend to be slightly longer.

Despite the statistical consistencies as described above, it should be taken into account that the condition  $K_{ij} \leq 0$  occurred in both the secular and direct integrations. The quantity  $K_{ij}$  is defined for two adjacent orbits  $i$  and  $j$ , with

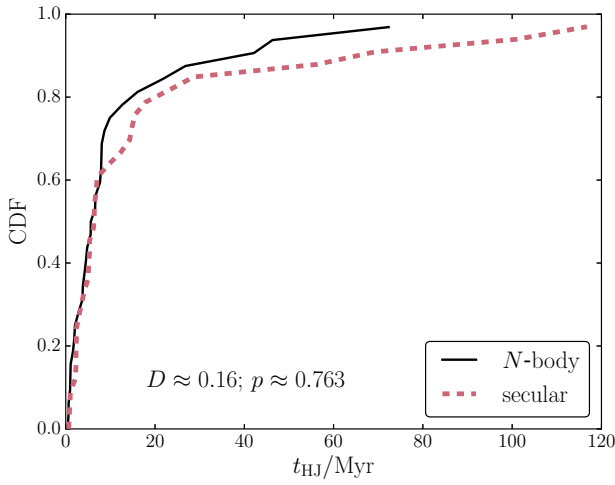


**Figure 2.** The CDF of the HJ formation times (see text for definition) according to ARCHAIN (black solid line) and to SECULARMULTIPLE (red dashed line). K-S test statistics are indicated.

$a_j > a_i$ , as

$$K_{ij} \equiv \frac{a_j(1-e_j) - a_i(1+e_i)}{R_{H;ij}}, \quad (1)$$

where

$$R_{H;ij} \equiv \frac{a_i + a_j}{2} \left( \frac{m_i + m_j}{3M_\star} \right)^{1/3} \quad (2)$$

is the mutual Hill radius. With SECULARMULTIPLE,  $K_{ij} \leq 0$  occurred for  $\approx 0.00016$  and  $\approx 0.021$  of all output times for orbit pairs (1, 2) and (2, 3), respectively. With ARCHAIN, these fractions were  $\approx 0.0002$  and  $\approx 0.015$ , for the same orbit pairs. If  $K_{ij} \leq 0$ , then the assumptions on which the secular method is based formally break down, and results should be interpreted critically. In our population synthesis study (Section 4), integrations were stopped at occurrences of  $K_{ij} \leq 0$ . To investigate whether this affects our conclusions, some of the integrations were not stopped when  $K_{ij} \leq 0$ .

#### 4 POPULATION SYNTHESIS

We used SECULARMULTIPLE to compute the dynamical evolution of a population of multiplanet systems with three to five planets. The innermost planet was initially located between 1 and 4 AU commensurate with planet formation just beyond the snow line. Taking into account tidal evolution, we focus on the orbital evolution of the innermost planet in the context of WJs and HJs.

##### 4.1 Initial conditions

To generate the initial conditions of our systems, we used a combination of grid and Monte Carlo sampling. We defined a grid with the following parameters: (1) the viscous timescale  $t_{V,1}$  of the innermost planet, (2) the number of planets  $N_p$ , (3)  $\beta$ , which is related to the rms width of the initial

inclination and eccentricity distribution (see below), and (4) the radius of the innermost planet,  $R_1$ . The following values were considered:

$$\begin{cases} t_{V,1} \in \{10^{-2}, 10^{-1}, 10^0\} t_{V,SKD}; \\ N_p \in \{3, 4, 5\}; \\ \beta \in \left\{ \left(20 \frac{\pi}{180}\right)^{-2}, \left(15 \frac{\pi}{180}\right)^{-2}, \left(10 \frac{\pi}{180}\right)^{-2} \right\} \\ \approx \{8.2, 14.6, 32.8\}; \\ R_1 \in \{1.0, 1.5\} R_J. \end{cases} \quad (3)$$

For gas giant planets and high- $e$  migration, Socrates et al. (2012) provided the constraint  $t_{V,1} \lesssim 1.2 \times 10^4$  hr, by requiring that a HJ at 5 d is circularized in less than 10 Gyr. We adopted a reference value  $t_{V,SKD} = 1.2 \times 10^4$  hr  $\approx 1.37$  yr, and considered  $t_{V,1}$  corresponding to 1, 10 and 100 times more efficient tides compared to  $t_{V,SKD}$ . The viscous timescale  $t_{V,SKD}$  corresponds to a tidal quality factor of  $Q_1 \approx 1.1 \times 10^5$  (cf. equation 37 from Socrates et al. 2012), and  $Q_1 \propto t_{V,1}$ .

We considered two planetary radii of 1 and  $1.5 R_J$ . Large planetary radii might be expected because of inflation due to tidal heating.

For each of the 54 combinations of grid parameters, we sampled  $N_{MC} = 1000$  systems using the following approach. The masses  $m_i$  of the  $N_p$  planets were sampled from flat distributions with  $0.5 M_J < m_i < 5 M_J$ . The inclinations  $i_i$  (as measured in radians, and defined with respect to an arbitrary reference plane) and eccentricities  $e_i$  of the planetary orbits were both sampled from a Rayleigh distribution,

$$\frac{dN}{dx} \propto x \exp(-\beta x^2), \quad (4)$$

where  $\beta = \langle x^2 \rangle^{-1}$  (assuming  $0 < x < \infty$ ) characterises the width of the distribution. The sampling limits were  $0 < e_i < 0.8$  and  $0^\circ < i_i < 30^\circ$ . The arguments of pericenter  $\omega_i$  and the longitudes of the ascending nodes  $\Omega_i$  were sampled from flat distributions between  $0^\circ$  and  $360^\circ$ .

The semimajor axes of the planets  $a_i$  were sampled from flat distributions, with the fixed ranges

$$\begin{cases} 1.0 \text{ AU} < a_1 < 4.0 \text{ AU}; \\ 6.0 \text{ AU} < a_2 < 10.0 \text{ AU}; \\ 15.0 \text{ AU} < a_3 < 30.0 \text{ AU}; \\ 35.0 \text{ AU} < a_4 < 50.0 \text{ AU}; \\ 60.0 \text{ AU} < a_5 < 100.0 \text{ AU}. \end{cases} \quad (5)$$

These choices are somewhat arbitrary. The semimajor axes of planets beyond  $\sim 5$  AU are still poorly constrained by observations. Assumptions must therefore be made regarding the semimajor axes, in particular for orbits outside of the innermost planet. The ranges of  $a_1$ ,  $a_2$  and  $a_3$  are similar to the values that were assumed by Wu & Lithwick (2011) (1, 6 and 16 AU, respectively). The choice of a flat distribution, apart from its simplicity, is motivated by the ability to easily disentangle any dependence of the results on the semimajor axes. At any rate, it should be taken into account that our choice of the initial semimajor axes is not unique, and likely affects the results of the population synthesis.

We rejected a sampled combination of  $m_i$ ,  $a_i$  and  $e_i$  if  $K_{ij} < K_0 \equiv 2$  for any adjacent pair  $(i, j) = (i, i+1)$  of orbits (cf. equation 1). The specific value of  $K_0$  is arbitrary. Choosing the value  $K_0 = 0$  would produce a large fraction of systems in which the secular method is questionable from the start (cf. Section 3), whereas a large value of

$K_0$ , say  $K_0 = 12$ , would produce too-well-separated systems in which the eccentricities would hardly evolve, and no WJs or HJs would be formed. As a compromise, we set  $K_0 = 2$ .

For the other (non-sampled) initial parameters, we refer to the last column of Table 1.

## 4.2 Stopping conditions

The integrations were stopped if one of the following conditions was met.

- (i) The integration time reached 10 Gyr.
- (ii) A HJ was formed, i.e.  $P_1 < 10$  d and  $e_1 < 10^{-3}$ . The orbit is then well within the regime of the decoupling of tidal from secular evolution, and there is no further tidal evolution since the orbit is (essentially) circularised.
- (iii) The innermost planet was tidally disrupted by the star, i.e.  $r_{p,1} = a_1(1 - e_1) < r_t$ , where  $r_t$  is given by

$$r_t = \eta R_1 \left( \frac{M_\star}{m_1} \right)^{1/3}. \quad (6)$$

Here,  $\eta$  is a dimensionless parameter; throughout, we assumed  $\eta = 2.7$  (Guillochon et al. 2011).

(iv) The condition  $K_{ij} \leq 0$  (cf. equation 1) occurred for any pair of adjacent orbits  $(i, j)$ , i.e. the secular approximation formally broke down. We also carried out additional simulations for some parameter combinations without this stopping condition to investigate the sensitivity of our results on this condition.

(v) The run time of the simulation exceeded 4 CPU hours (imposed for practical reasons).

## 4.3 Results

### 4.3.1 Overview

Our results are summarised in Table 2. For each combination of  $t_{V,1}$ ,  $N_p$ ,  $\beta$  and  $R_1$ , we list the fractions with respect to the  $N_{MC} = 1000$  Monte Carlo-sampled systems of the following outcomes, closely related to the stopping conditions.

- (i) No migration occurred, i.e. the final orbital period  $P_1 > 100$  d ( $f_{\text{no migration}}$ ).
- (ii) A HJ was formed ( $f_{\text{HJ}}$ ; WJs: see below).
- (iii) The innermost planet was tidally disrupted ( $f_{\text{TD}}$ ).
- (iv)  $K_{ij} \leq 0$  occurred for any orbit pair ( $f_{K_{ij} \leq 0}$ ).
- (v) The maximum run time of 4 CPU hours was exceeded ( $f_{\text{run time exceeded}}$ ).

These fractions are given after either 5 or 10 Gyr of integration, or by sampling a random time between 100 Myr and 10 Gyr for each of the systems, corresponding to a constant star formation rate (indicated with  $t_x$  in the table; output times were separated by 100 Myr). For  $t_{V,1} = 10^{-2} t_{V,\text{SKD}}$  and  $R_1 = 1 R_J$ , when most HJs are formed, we also carried out simulations without the  $K_{ij} \leq 0$  stopping condition. These can be recognised in Table 2 with the entries with  $f_{K_{ij} \leq 0}$  marked as –.

The fractions of HJs formed are typically low; the largest fraction is 0.007, obtained after 10 Gyr for the set of simulations with  $t_{V,1} = 0.01 t_{V,\text{SKD}}$ ,  $N_p = 4$ ,  $\beta \approx 8.2$  and  $R_1 = 1 R_J$ . In contrast, the fraction of tidal disruptions is

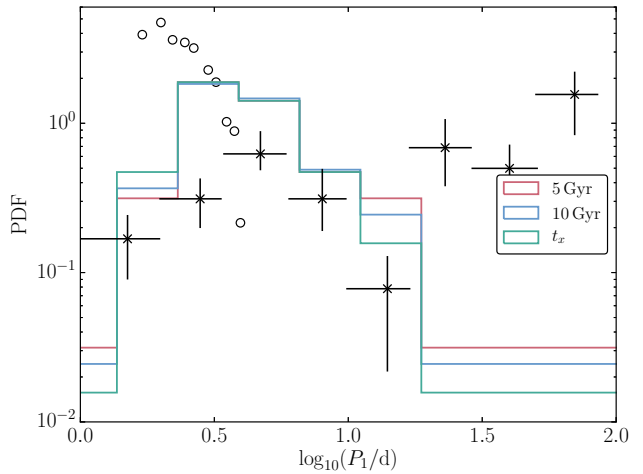


**Figure 3.** Solid lines: the distributions of the orbital period of the innermost planet at 5 and 10 Gyr, and at a random time ( $t_x$ ). Crosses: observations from Santerne et al. (2016); error bars are indicated with black lines. Open circles: distribution from Fig. 23 of Anderson et al. (2016) for  $M_p = 1 M_J$  and  $\chi = 100$ . Distributions are normalised to unit total area.

much larger, typically a few per cent, and reaching values of  $\approx 0.2 - 0.3$  for  $N_p = 5$ .

The number of WJs (defined as planets with an orbital period between 10 and 100 days at a given time) is even smaller than the number of HJs, and the associated fractions are not included in Table 2. Among the 54,000 integrations, 34 HJs were formed after 10 Gyr, whereas the number of WJs at that time is 2 (the number of WJs and HJs at 5 Gyr is 2 and 26, respectively). Moreover, the semimajor axes of these 2 WJs are  $\approx 0.1$  AU, i.e. the WJs are on the ‘hot’ end of the WJ spectrum, and near the (not well-defined) boundary between WJs and HJs.

For larger values of  $t_{V,1}$ , i.e. for weaker tidal dissipation strength in the innermost planet, no HJs are formed at all, for any of the combinations of the grid parameters. Note that the number of Monte Carlo realisations per parameter combination was limited to  $N_{MC} = 1000$ , implying that the HJ fractions could be less than 0.001, but nonzero. Also, uncertainties associated with the stopping condition  $K_{ij} \leq 0$  and premature terminations of the integrations because of the exceeding of the maximum run time, should be taken into account. These are discussed in more detail in Section 5.1.

Note that the cumulative ‘non-migrating’ fractions in Table 2 are typically lower compared to the fraction of HJs found in Section 3. This can be attributed to the high initial eccentricities and inclinations that were assumed in Section 3, of  $\approx 0.5$ , whereas they were typically lower in the population synthesis.

### 4.3.2 Final orbital period distributions

In Fig. 3, we show the distributions of the orbital periods of the innermost planet at various times, combining results from all parameter combinations. With the solid lines, we

$t_{V,1}$	$N_p$	$\beta$	$R_1$	$f_{\text{no migration}}$												$f_{\text{HJ}}$												$f_{\text{TD}}$												$f_{K_{ij} \leq 0}$												$f_{\text{run time exceeded}}$																																																																																																																																																																																																																																																																																																																																																																																																																																																																																																																																																																																																																																																																																																																																																																																																																									
				$t_{\text{end}}$ (Gyr) $\rightarrow$			5			10			$t_x$			5			10			$t_x$			5			10			$t_x$			5			10			$t_x$			5			10			$t_x$			5			10			$t_x$			5			10			$t_x$			5			10			$t_x$			5			10			$t_x$			5			10			$t_x$			5			10			$t_x$			5			10			$t_x$			5			10			$t_x$			5			10			$t_x$			5			10			$t_x$			5			10			$t_x$			5			10			$t_x$			5			10			$t_x$			5			10			$t_x$			5			10			$t_x$			5			10			$t_x$			5			10			$t_x$			5			10			$t_x$			5			10			$t_x$			5			10			$t_x$			5			10			$t_x$			5			10			$t_x$			5			10			$t_x$			5			10			$t_x$			5			10			$t_x$			5			10			$t_x$			5			10			$t_x$			5			10			$t_x$			5			10			$t_x$			5			10			$t_x$			5			10			$t_x$			5			10			$t_x$			5			10			$t_x$			5			10			$t_x$			5			10			$t_x$			5			10			$t_x$			5			10			$t_x$			5			10			$t_x$			5			10			$t_x$			5			10			$t_x$			5			10			$t_x$			5			10			$t_x$			5			10			$t_x$			5			10			$t_x$			5			10			$t_x$			5			10			$t_x$			5			10			$t_x$			5			10			$t_x$			5			10			$t_x$			5			10			$t_x$			5			10			$t_x$			5			10			$t_x$			5			10			$t_x$			5			10			$t_x$			5			10			$t_x$			5			10			$t_x$			5			10			$t_x$			5			10			$t_x$			5			10			$t_x$			5			10			$t_x$			5			10			$t_x$			5			10			$t_x$			5			10			$t_x$			5			10			$t_x$			5			10			$t_x$			5			10			$t_x$			5			10			$t_x$			5			10			$t_x$			5			10			$t_x$			5			10			$t_x$			5			10			$t_x$			5			10			$t_x$			5			10			$t_x$			5			10			$t_x$			5			10			$t_x$			5			10			$t_x$			5			10			$t_x$			5			10			$t_x$			5			10			$t_x$			5			10			$t_x$			5			10			$t_x$			5			10			$t_x$			5			10			$t_x$			5			10			$t_x$			5			10			$t_x$			5			10			$t_x$			5			10			$t_x$			5			10			$t_x$			5	

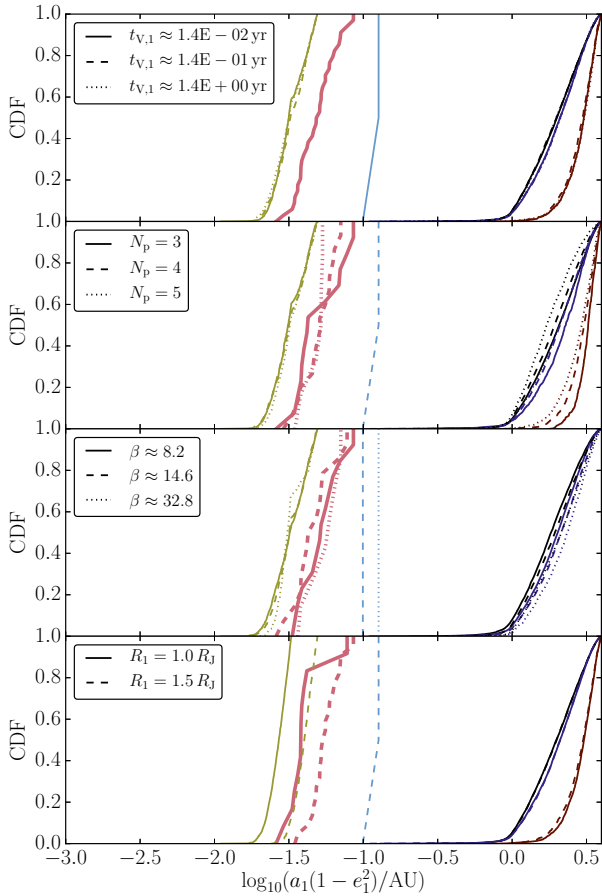


**Figure 4.** The innermost orbit semilatus rectum distributions after 10 Gyr (or after a stopping condition was met) plotted for different slices of the parameter space. In each panel, distributions are shown for all parameters combined, except one (different line styles). The varying parameters are  $tv,1$ ,  $N_p$ ,  $\beta$  and  $R_1$  in the top through bottom panels, respectively. Different types of systems are indicated with different colours: systems with no migration (black), HJs (light red), WJs (light blue), tidally disrupted inner planets (yellow),  $K_{ij} \leq 0$  (dark blue) or exceeding of run time (dark red).

#### 4.3.3 Dependence on the grid parameters

In Fig. 3, we combined results for all parameters. Here, we consider in more detail the dependence of the results on the individual parameters.

In Fig. 4, the innermost orbit semilatus rectum distributions after 10 Gyr (or after a stopping condition was met) are plotted for different slices of the parameter space. Considering tidal evolution only, the final semimajor axis (at the moment of circularisation) is expected to be equal to the semilatus rectum. In each panel, distributions are shown for all parameters combined, except one (different line styles). In addition, we distinguish between the different types of systems: no migration (black), HJs (light red), WJs (light

blue), tidally disrupted inner planets (yellow),  $K_{ij} \leq 0$  (dark blue) or exceeding of run time (dark red).

In the top panel, we show the dependence on  $tv,1$ . The distributions for non-HJ and non-WJ forming systems are essentially independent of  $tv,1$ . HJs (and WJs) are only formed for the smallest viscous time-scale of  $\approx 1.4 \times 10^{-2}$  yr. The requirement of highly efficient tides for HJ production was also found for other high-e migration scenarios, in particular in stellar binaries (Petrovich 2015a).

The dependence on the number of planets and  $\beta$  is shown in the second and third panels of Fig. 4, respectively. Despite the expected propensity of exciting higher eccentricities with a larger number of planets and/or smaller  $\beta$ , the dependence of the semilatus rectum distributions on these parameters is weak.

The dependence on the radius of the innermost planet is shown in the bottom panel of Fig. 4. For HJs, the final semilatus rectum is smaller for smaller radii (see e.g. equation 3 of Wu & Lithwick 2011). For the tidally disrupted planets, a larger radius corresponds to a larger tidal disruption radius (cf. equation 6), and therefore a larger semilatus rectum at the moment of disruption.

#### 4.3.4 Dependence on the initial orbital properties

In Fig. 5, we show how the various outcomes in our simulations depend on the initial semimajor axes (left column) and the eccentricities (right column), for the three innermost orbits. We recall that the semimajor axes were sampled linearly from fixed ranges, whereas the eccentricities were sampled from a Rayleigh distribution with various widths expressed by  $\beta$  (cf. Section 4.1).

The largest differences in the initial semimajor axes between the various outcomes are apparent in the innermost orbit. The distribution of the initial  $a_1$  for the HJ and tidal disruption systems is skewed towards small values compared to the other systems, with  $a_1 \lesssim 2$  AU for most ( $\approx 0.95$  and  $\approx 0.8$ , respectively) of the systems. This can be attributed to two effects. For the typical  $a_2$  and  $a_3$  in the simulations, a small  $a_1$  implies a larger commensurability between the LK time-scales associated with orbit pairs (1,2) and (2,3), and therefore more likely chaotic evolution and higher eccentricities (e.g. Hamers et al. 2015). Also, the required eccentricities for small pericenter distances (important for tidal dissipation or tidal disruption) are lower for smaller semimajor axes.

The systems with exceeded run times (dark red lines) preferentially have large  $a_1$ , whereas  $a_2$  is preferentially small. These systems are unlikely to result in HJs, cf. Section 5.1. With regard to the other orbits and outcomes, no clear differences can be discerned in the initial distributions of the semimajor axes.

HJ and tidal disruption systems typically show a preference for initially higher values of the eccentricities, notably  $e_2$ . Otherwise, there is no strong dependence on the initial eccentricities.

Observations of companions planets to HJs are currently still strongly limited. In the latest surveys, detections of Jupiter-mass planets are only 100% complete for planets out to  $\approx 10$  AU (Bryan et al. 2016). In our simulations, except for the innermost two planets, the orbits span a much larger range in semimajor axis. Despite the incom-

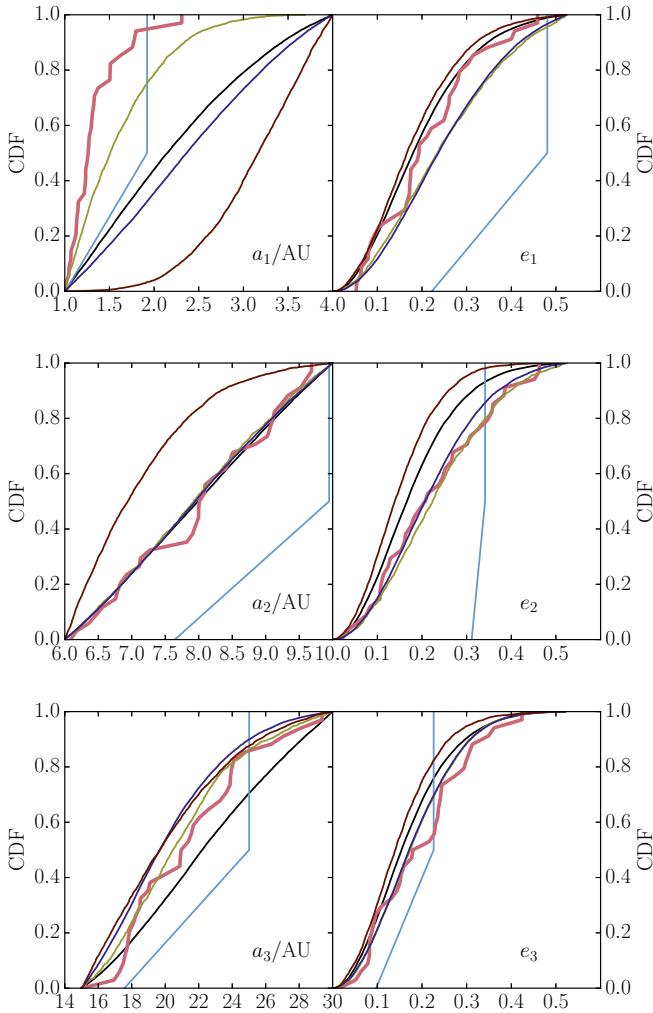


**Figure 5.** The initial distributions of the semimajor axes (left column) and the eccentricities (right column) for the various outcomes of the Monte Carlo simulations. Colors indicate systems with no migration (black), HJs (light red), WJs (light blue), tidally disrupted inner planets (yellow),  $K_{ij} \leq 0$  (dark blue) or exceeding of run time (dark red).

completeness of the observations, we show in Fig. 6 observed distributions of the semimajor axes (top panel) and the eccentricities (bottom panel) for planets with  $m_1 \sin(i) > 0.1 M_J$  obtained from the *Open Exoplanet Catalogue*. We consider multiplanet systems with at least two observed planets, and make a distinction between systems with the innermost observed orbit  $a_1 < 1$  AU (solid lines) and  $a_1 > 1$  AU (dashed lines). Some difference can be seen in the distributions of  $a_2$  for the two populations with  $a_1 < 1$  AU and  $a_1 > 1$  AU:  $a_2$  tends to be smaller for the former population. This trend is not reflected in our simulations (cf. the second row of Fig. 5). With regard to  $a_3$ , there seems to be a large difference in the distribution of  $a_3$  for the two populations. However, our observational sample only includes 5 systems with at least 3 planets, so with this low number of systems this difference cannot be considered significant.

Another, more theoretically oriented, quantity is the

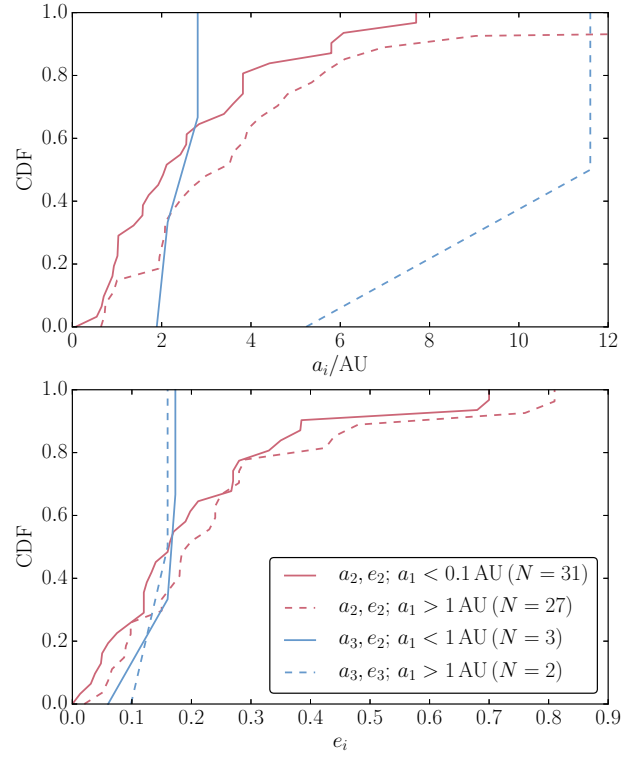


**Figure 6.** Observed distributions of the semimajor axes (top panel) and the eccentricities (bottom panel) for planets with  $m_1 \sin(i) > 0.1 M_J$  obtained from the *Open Exoplanet Catalogue*. We consider multiplanet systems with at least two observed planets, and make a distinction between systems with the innermost observed orbit  $a_1 < 1$  AU (solid lines) and  $a_1 > 1$  AU (dashed lines).

angular-momentum deficit (AMD). The AMD is defined as

$$\text{AMD} = \sum_{i=1}^{N_p} m_i \sqrt{a_i} \left[ 1 - \sqrt{1 - e_i^2} \cos(i_{\text{var},i}) \right], \quad (7)$$

where  $i_{\text{var},i}$  is the inclination with respect to the invariable plane, i.e. the plane perpendicular to the total orbital angular-momentum vector of the system. In terms of the AMD, high eccentricities and/or chaotic motion can be achieved if  $\text{AMD} \gtrsim m_1 \sqrt{a_1}$  (Wu & Lithwick 2011; Lithwick & Wu 2011, 2014).

In our simulations, there is indeed a strong dependence on the AMD. In Fig. 7, we show the initial distributions of the AMD for the various outcomes. Of the non-migrating systems (black line), nearly all ( $\approx 0.99$ ) have an AMD which is  $< m_1 \sqrt{a_1}$ . In contrast, all disrupted systems (yellow line) have an AMD  $\gtrsim m_1 \sqrt{a_1}$ , and the HJ systems (light red line) have an AMD  $\gtrsim 0.8 m_1 \sqrt{a_1}$ , with the majority ( $\sim 0.8$ ) of systems having  $\text{AMD} > m_1 \sqrt{a_1}$ .

The systems in which  $K_{ij} \leq 0$  occurred (dark blue line) have higher AMD compared to the non-migrating systems, which can be attributed to the higher eccentricities attained with higher AMDs, therefore more likely leading to  $K_{ij} \leq 0$ .

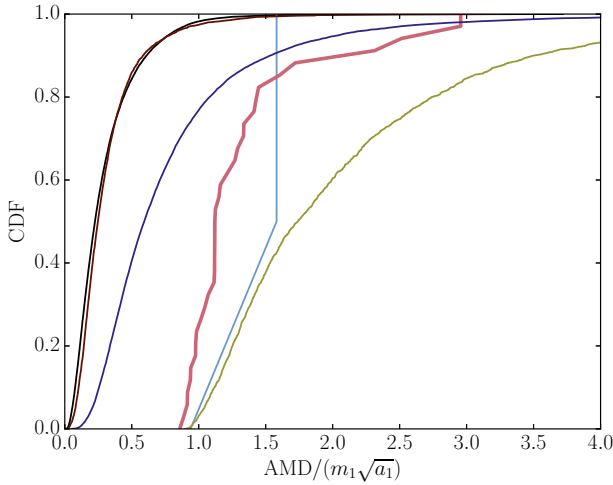


**Figure 7.** The initial distributions of the AMD for the various outcomes of the Monte Carlo simulations. Colors indicate systems with no migration (black), HJs (light red), WJs (light blue), tidally disrupted inner planets (yellow), orbit crossings (dark blue) or exceeding of run time (dark red).

Nonetheless,  $\approx 0.8$  of these systems have  $< m_1 \sqrt{a_1}$ , indicating that the majority of systems with  $K_{ij} \leq 0$  would not have produced HJs or tidally disrupted planets if the stopping condition at  $K_{ij} \leq 0$  had not been imposed. This is consistent with the result that the HJ fractions are not strongly affected in the runs without this stopping condition (cf. Table 2 and Section 4.3.1).

There are distinct differences with respect to the AMD between the HJ and tidal disruption systems. Most ( $\approx 0.9$ ) of the HJs have  $\text{AMD} < 1.5 m_1 \sqrt{a_1}$ , whereas for the tidal disruption systems this fraction is markedly lower,  $\approx 0.4$ . The preference for the tidal disruption systems for higher AMDs can be explained by the higher eccentricities reached in the innermost orbit, therefore more likely resulting in the (immediate) tidal disruption of the innermost planet, rather than tidal dissipation, which requires a certain amount of time to dissipate energy and reduce the eccentricity. This implies that there is a ‘window’ for producing HJs through secular evolution: the AMD should be large enough to excite high eccentricities, but small enough to prevent violent excitation of the eccentricities leading to tidal disruption before tidal dissipation can be effective.

#### 4.3.5 Mass dependence

The orbits of lower-mass planets carry less orbital angular momentum compared to higher-mass counterparts, making the former more susceptible to angular-momentum exchanges with orbits of other planets. Therefore, secular eccentricity excitation is expected to be more pronounced if the outer planets are more massive than the innermost planet. In our simulations, we assumed a flat distribution of the planetary masses between  $0.5$  and  $5 M_J$ .

In the top panels of Fig. 8, we show the distributions of the mass of the innermost planet for the various outcomes in the simulations. For the non-migrating systems,

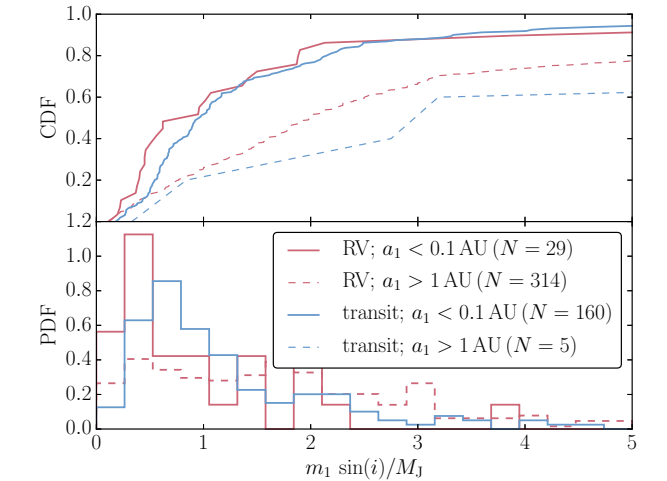
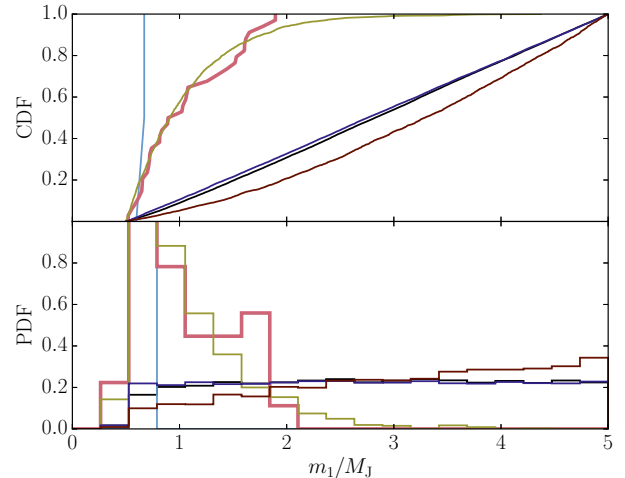


**Figure 8.** Top panels: distributions of the initial mass of the innermost planet for the Monte Carlo simulations with all grid parameters combined. Different types of systems are indicated with different colours: systems with no migration (black), HJs (light red), WJs (blue), tidally disrupted inner planets (yellow),  $K_{ij} \leq 0$  (dark blue) or exceeding of run time (dark red). Bottom panels: the observed mass distributions of planets with  $m_1 \sin(i) > 0.1 M_J$  (obtained from the *Open Exoplanet Catalogue*). Two discovery methods are included: RV (red) and transit (blue). Also, a distinction is made between the semimajor axis:  $a_1 < 0.1 \text{ AU}$  (solid lines) and  $a_1 > 1 \text{ AU}$  (dashed lines).

the mass distribution is consistent with a flat distribution, reflecting the initial distribution, and showing no mass preference. For HJ and tidal disruption systems, the mass distributions are different. For the latter groups, there is a preference for lower-mass planets, with  $m_1 \lesssim 0.9 M_J$  for  $\sim 0.5$  of the systems. There are no HJs, and few tidal disruption systems with  $m_1 \gtrsim 2 M_J$ . This implies a clear quantitative prediction for high- $e$  migration in multiplanet systems, and which was given qualitatively in Wu & Lithwick (2011): the HJ should have a typical (median) mass of  $\sim 1 M_J$ , and not be more massive than  $\sim 2 M_J$ .

Observations show a deficit of massive HJs (Zucker & Mazeh 2002; Udry & Santos 2007), which

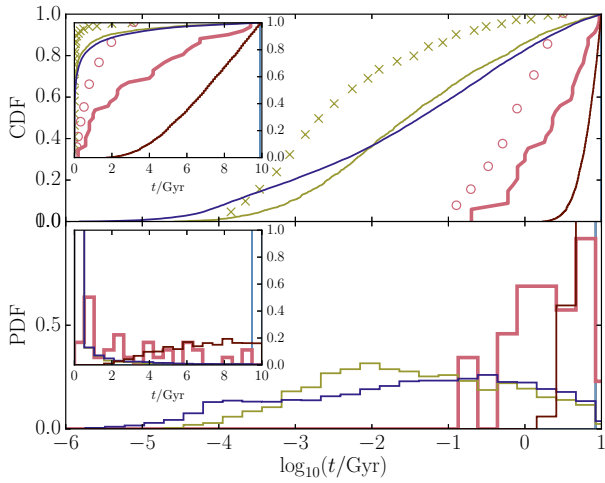


**Figure 9.** The final times associated with the various outcomes in our population synthesis (with all parameters combined). For systems in which a stopping condition occurred, these final times are the age of the system when the integration was stopped. In the case of HJs (light red lines), these times are the times of HJ formation. Different types of systems are indicated with different colours: systems with no migration (black), HJs (light red), WJs (blue), tidally disrupted inner planets (yellow),  $K_{ij} \leq 0$  (dark blue) or exceeding of run time (dark red). The same data, shown using linear scales on the abscissa, is shown in the insets. Red open circles and yellow crosses: data for HJs and tidal disruptions, respectively, from the second panel of Fig. 22 ( $M_p = 1 M_J$ ) of Anderson et al. (2016).

seems consistent with the above prediction. More quantitatively, the observed mass distributions of planets with  $m_1 \sin(i) > 0.1 M_J$  (obtained from the *Open Exoplanet Catalogue*) are shown in the bottom panels of Fig. 8. We made a distinction between discovery method (RV or transit) and semimajor axis ( $a_1 < 0.1$  AU and  $a_1 > 1$  AU). The planets from the RV observations within 0.1 AU are typically of lower mass compared to planets at  $> 1$  AU. This trend is consistent with the predictions as described above. However, one should be cautious when ascribing the observed mass difference to secular evolution alone, given that the latter unlikely produces all HJs, and the observed mass distribution is also likely affected by other processes, such as primordial ‘mass segregation’, whereas in the simulations we assumed an initially flat distribution. Moreover, the RV observations are biased, because planets at  $> 1$  AU are more easily detected if they are more massive.

#### 4.3.6 HJ formation times

As mentioned in Section 1, secular evolution in multiplanet systems typically occurs on long time-scales of order Gyr, implying that HJs formed through this mechanism could have been deposited at their current orbit at late stages in the MS life-time of the host star. In Fig. 9, we show the ‘final’ times associated with the various outcomes in our population synthesis (with all parameters combined). For systems in which a stopping condition occurred, these final times are the age of the system when the integration was

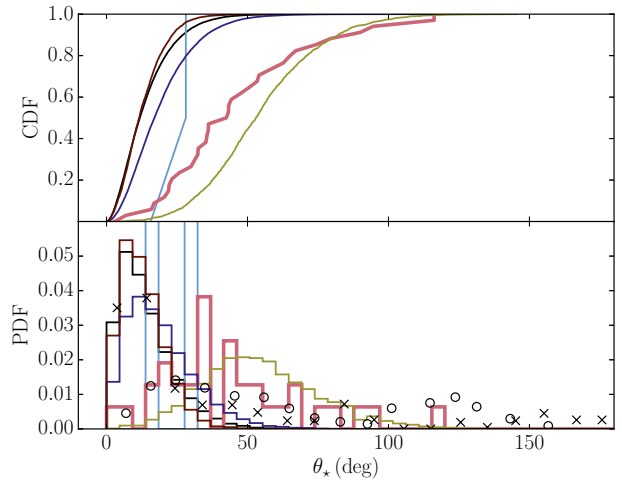


**Figure 10.** Distributions after 10 Gyr (or after a stopping condition) of the stellar obliquity  $\theta_\star$  for the Monte Carlo simulations with all grid parameters combined. As in Fig. 4, different types of systems are indicated with different colours: systems with no migration (black), HJs (light red), WJs (blue), tidally disrupted inner planets (yellow),  $K_{ij} \leq 0$  (dark blue) or exceeding of run time (dark red). Open circles: distribution from Fig. 24 of Anderson et al. (2016) for  $M_p = 1 M_J$  and  $\chi = 100$ . Crosses: observed projected obliquity distribution, adopted from Lithwick & Wu (2014). The PDFs are normalised to unit total area.

stopped. In the case of HJs (light red lines), these times are the times of HJ formation, as defined in Section 4.2.

The HJs in our simulations are indeed formed late, with a median formation time of  $\approx 2$  Gyr, and with a fraction  $\approx 0.2$  of the HJs formed after  $\approx 6$  Gyr. These times are much longer compared to times associated with high- $e$  migration due to close encounters (Rasio & Ford 1996; Chatterjee et al. 2008; Ford & Rasio 2008; Jurić & Tremaine 2008), and also longer compared to those typically found for high- $e$  migration in stellar binaries (Anderson et al. 2016; cf. the red open circles in Fig. 9). In contrast, tidal disruptions occur much earlier, with  $\approx 0.85$  of the disruptions occurring before 1 Gyr.

#### 4.3.7 Stellar obliquity

In Fig. 10, we show, for all grid parameters combined, the distributions after 10 Gyr (or after a stopping condition) of the stellar obliquity, i.e. the angle between the stellar spin and the orbit of the innermost planet. Initially, the stellar spin and innermost orbit were assumed to be aligned, i.e. zero obliquity was assumed (cf. Table 1).

For high- $e$  migration scenarios with three bodies (or, more generally, LK cycles with tidal friction), it has been well established that the obliquity for HJs should be clustered around  $40^\circ$  and  $130^\circ$  (Fabrycky & Tremaine 2007; Naoz & Fabrycky 2014; Anderson et al. 2016). This can be explained intuitively by noting that during LK cycles, the eccentricity maxima occur at mutual inclinations of  $\approx 40^\circ$  or  $130^\circ$ , and mutual inclination tends to be ‘locked’ after the onset of strong tidal dissipation (this is assuming that

the stellar spin vector itself does not change due to spin-planet orbit coupling, see Storch et al. 2014; Storch & Lai 2015; Anderson et al. 2016). Observations have revealed a range of obliquities, depending on the stellar surface temperature (e.g. Winn et al. 2011; Mazeh et al. 2015).

In our simulations, we find that the obliquity distributions of the HJs and tidally disrupted planets are distinct from non-migrating systems. The obliquities of the former are broadly distributed between  $\sim 0^\circ$  and  $\sim 120^\circ$ , with some preference for obliquities around  $40^\circ$  (for HJs) or  $50^\circ$  (for tidal disruption systems). In contrast, the observed HJ obliquity distribution peaks around  $20^\circ$  (cf. the black crosses in Fig. 10).

There is no peak around  $130^\circ$ , as found e.g. by Anderson et al. (2016), who considered high- $e$  migration in stellar binaries (cf. the black open circles in Fig. 10). This can be attributed to the fact that in our simulations, the planets were always initially prograde, and there is no expected characteristic symmetric inclination for secular evolution in multiplanet systems. Nevertheless, we still find that  $\sim 0.1$  of the HJs systems have retrograde obliquities.

## 5 DISCUSSION

### 5.1 Uncertainties in the secular integrations

Here, we discuss uncertainties associated with the stopping condition  $K_{ij} \leq 0$  and premature terminations of the integrations because the run time exceeded our maximum set value (cf. Section 4.2).

A comparison of the HJ fractions between runs with and without the  $K_{ij} \leq 0$  stopping condition enabled in Table 2, shows that disabling the stopping condition results in different fractions. Typically, the fraction increases, which can be understood by noting that systems in which  $K_{ij} \leq 0$  occurs are likely to produce high eccentricities in the inner orbit, and therefore HJs. Nonetheless, the fractions remain small, not reaching values larger than 0.007, indicating that the result of small HJ fractions is robust. Nevertheless, it remains unclear how the results would be affected if  $N$ -body integrations were used, which evidently do not suffer from limitations associated with small or negative  $K_{ij}$ . This important aspect should be investigated in future work.

The systems in which the run time was exceeded show a strong preference for large initial  $a_1$ , typically  $a_1 \sim 3$  AU, and small  $a_2$ , typically  $a_2 \sim 7$  AU (cf. Fig. 5). This implies short secular time-scales in the innermost orbit. Consequently, the number of oscillations within the time span of 10 Gyr is very large, requiring much computation time and thus hitting our set limit of 4 CPU hours.

The fraction of systems in which the run time was exceeded typically increases with  $\beta$ . For large  $\beta$ , the initial eccentricities and inclinations are small, implying relatively weak secular excitation. This is also reflected by the AMD – systems in which the run time was exceeded typically have small AMD,  $\text{AMD} \lesssim m_1 \sqrt{a_1}$  (cf. Fig. 7). Also,  $m_1$  tends to be large, typically  $m_1 \sim 3 M_J$  (cf. Fig. 8).

The HJ systems, on the other hand, are associated with  $a_1 \lesssim 2$  AU and no strong preference for  $a_2$  (cf. Fig. 5), a small  $\beta$ , large AMD  $\gtrsim m_1 \sqrt{a_1}$  (cf. Fig. 7), and  $m_1 \lesssim 2 M_J$ . This suggests that the HJ fractions would likely not be very different if the stopping condition (v) had not been imposed.

### 5.2 HJ fraction and comparisons to other variants of high- $e$ migration

In our population synthesis simulations, the highest intrinsic HJ fraction obtained was 0.007, assuming  $t_{V,1} \approx 0.014$  yr. This corresponds to 100 times more efficient tides compared to  $t_{V,1} \approx 1.4$  yr, which would circularize a HJ at 5 days in less than 10 Gyr (Socrates et al. 2012). For the purposes of this section, we round this fraction to  $f_{\text{HJ,multi,sim}} = 0.01$ , and adopt this value as a maximum fraction.

Assuming a giant planet occurrence rate around MS stars of  $f_{\text{GP}} = 0.1$  and an optimistic multiplanet fraction of 1, we find a HJ fraction around MS stars of  $f_{\text{HJ,multi}} = f_{\text{HJ,multi,sim}} f_{\text{GP}} = 0.001$ . In contrast, the observed HJ fraction is  $f_{\text{HJ,obs}} \sim 0.01$  (e.g. Wright et al. 2012), an order of magnitude larger. We emphasize that higher HJ fractions would be obtained in simulations with even smaller values of  $t_{V,1}$  (i.e. even more efficient tides), and/or larger planetary radii  $R_1$ . Also, we (necessarily) made assumptions about the orbital configurations (most importantly the semimajor axes, eccentricities and inclinations), which also affect the simulated HJ fractions.

Our simulated HJ fraction of  $\sim 0.01$  is similar or slightly lower compared to studies of high- $e$  migration in two-planet or stellar binary systems. Anderson et al. (2016) find a fraction of  $f_{\text{HJ,bin,sim}} \sim 0.03$  for high- $e$  migration in stellar binaries. In Petrovich & Tremaine (2016), the two-planet case is considered, and  $f_{\text{HJ,two-p,sim}} = 0.051$  is found for  $t_{V,1} = 1.4$  yr. The high fraction in the latter paper may be due to higher assumed initial inclinations and more compact systems (smaller  $a_2/a_1$ ) compared to our simulations. The two-planet case is also considered by Antonini et al. (2016), who find  $f_{\text{HJ,two-p,sim}} = 0.01$  for  $t_{V,1} = 1.4$  yr.

## 6 CONCLUSIONS

We have studied the orbital migration of Jupiter-like planets induced by secular interactions in multiplanet systems (three to five planets), resulting in HJs. In this variant of high- $e$  migration, the eccentricity of the orbit of the innermost planet is excited to high values on secular time-scales (order Gyr). Combined with tidal dissipation, which is highly effective for high eccentricities, this can produce a Jupiter-like planet in a tight orbit. Our conclusions are as follows.

1. For a set of three-planet systems we have shown that the secular code SECULARMULTIPLE (Hamers & Portegies Zwart 2016) produces results that are statistically consistent with those of more accurate direct  $N$ -body integrations (Section 3).
2. We carried out a population synthesis study of multiplanet systems with SECULARMULTIPLE, taking into account tidal dissipation in the innermost planet and the central star (Section 4). We found HJ fractions of at most 0.007, assuming  $t_{V,1} \approx 0.014$  yr. This corresponds to 100 times more efficient tides compared to  $t_{V,1} \approx 1.4$  yr, for which a HJ at 5 d would circularize in less than 10 Gyr (Socrates et al. 2012). For weaker tidal dissipation ( $t_{V,1}$  larger than  $\approx 0.014$  yr), we found no HJs. Larger fractions would be obtained for even lower values of the innermost planet viscous time-scale (stronger tides), i.e.  $t_{V,1} < 1.4 \times 10^{-2}$  yr. The

HJ fractions are similar or lower compared to other variants of high- $e$  migration, but this comparison depends strongly on the initial conditions, such as the initial semimajor axes, eccentricities and inclinations.

3. In the population synthesis, we found that in up to  $\sim 0.3$  of the systems, the innermost planet is tidally disrupted. The large proportion of tidally disrupted planets to HJs can be explained qualitatively by noting that the eccentricity of the innermost orbit can be violently excited in multiplanet systems, implying that the planet is rapidly tidally disrupted before tidal dissipation is able to shrink and circularise the orbit. The large fraction of tidal disruptions in some of our simulations suggests that tidal disruptions in multiplanet systems, even if not extremely compact, could be common. For non-compact planetary systems, this suggests a possible difference in metallicity between stars with two or fewer planets, compared to stars with three or more planets.

4. The orbital period distribution of the HJs in our simulations is strongly peaked around  $\sim 5$  d, which coincides with the peak in the observed orbital period distribution of gas giant planets. The location of the peak is affected by the assumed tidal dissipation efficiency and the planetary radius. In our simulations, HJs with the longest periods correspond to an inflated planet with radius  $R_1 = 1.5 R_J$ . No planets were found in the simulations with orbital periods in the ‘period valley’ between 10 and 100 d, whereas observations show a significant population of planets in this regime, i.e. WJs. It is unlikely that WJs are produced through secular evolution in multiplanet systems, unless tidal dissipation is extremely efficient. Other high- $e$  migration scenarios also fail to produce WJs in the observed proportion (Petrovich & Tremaine 2016; Antonini et al. 2016). Alternative candidates for the origin of WJs are *in situ* formation or disk migration.

5. Our simulated HJs and tidally disrupted planets are preferentially not massive, i.e.  $m_1 \lesssim 2 M_J$ , with a median value of  $\approx 1 M_J$  (cf. Section 4.3.5), which is similar to observations. The stellar obliquity distribution is fairly uniform between  $\sim 0^\circ$  and  $\sim 120^\circ$  with some preference for obliquities around  $40^\circ$ . There is no peak at  $\sim 130^\circ$ , as opposed to high- $e$  migration in stellar binary or 2-planet systems (cf. Section 4.3.7). Approximately 0.1 of the HJs have retrograde obliquities.

6. Another characteristic of HJs formed in our simulations relevant for observations is the late formation time of up to  $\sim 10$  Gyr (cf. Section 4.3.6). This is in stark contrast to disk migration, for which formation is expected to occur within the first few Myr. Also, this characteristic can potentially distinguish between other variants of high- $e$  migration, which typically predict shorter formation times.

## ACKNOWLEDGEMENTS

This work was supported by the Netherlands Research Council NWO (grants #639.073.803 [VICI], #614.061.608 [AMUSE] and #612.071.305 [LGM]) and the Netherlands Research School for Astronomy (NOVA). We acknowledge the use of the astrix computer cluster of the national Israeli astrophysics I-CORE center. HBP acknowledges support from European union career integration grant ‘GRAND’, the

Minerva center for life under extreme planetary conditions and the Israel science foundation excellence center I-CORE grant 1829. YL acknowledges NSF grants AST-1109776 and AST-1352369 and NASA grant NNX14AD21G.

## References

Anderson K. R., Storch N. I., Lai D., 2016, *MNRAS*, **456**, 3671  
 Antonini F., Hamers A. S., Lithwick Y., 2016, preprint, ([arXiv:1604.01781](https://arxiv.org/abs/1604.01781))  
 Batygin K., Bodenheimer P. H., Laughlin G. P., 2015, preprint, ([arXiv:1511.09157](https://arxiv.org/abs/1511.09157))  
 Bodenheimer P., Hubickyj O., Lissauer J. J., 2000, *Icarus*, **143**, 2  
 Bryan M. L., et al., 2016, *ApJ*, **821**, 89  
 Chatterjee S., Ford E. B., Matsumura S., Rasio F. A., 2008, *ApJ*, **686**, 580  
 Eggleton P. P., Kiseleva L. G., Hut P., 1998, *ApJ*, **499**, 853  
 Fabrycky D., Tremaine S., 2007, *ApJ*, **669**, 1298  
 Ford E. B., Rasio F. A., 2008, *ApJ*, **686**, 621  
 Goldreich P., Tremaine S., 1980, *ApJ*, **241**, 425  
 Guillot J., Ramirez-Ruiz E., Lin D., 2011, *ApJ*, **732**, 74  
 Hamers A. S., Portegies Zwart S. F., 2016, *MNRAS*, **459**, 2827  
 Hamers A. S., Perets H. B., Antonini F., Portegies Zwart S. F., 2015, *MNRAS*, **449**, 4221  
 Harrington R. S., 1968, *AJ*, **73**, 190  
 Jurić M., Tremaine S., 2008, *ApJ*, **686**, 603  
 Knutson H. A., et al., 2014, *ApJ*, **785**, 126  
 Kolmogorov A., 1933, *G. Ist. Ital. Attuari*, **4**, 83  
 Kozai Y., 1962, *AJ*, **67**, 591  
 Laskar J., Gastineau M., 2009, *Nature*, **459**, 817  
 Lee E. J., Chiang E., Ormel C. W., 2014, *ApJ*, **797**, 95  
 Lidov M. L., 1962, *Planet. Space Sci.*, **9**, 719  
 Lin D. N. C., Papaloizou J., 1986, *ApJ*, **309**, 846  
 Lin D. N. C., Bodenheimer P., Richardson D. C., 1996, *Nature*, **380**, 606  
 Lithwick Y., Wu Y., 2011, *ApJ*, **739**, 31  
 Lithwick Y., Wu Y., 2014, *Proceedings of the National Academy of Science*, **111**, 12610  
 Mazer T., Perets H. B., McQuillan A., Goldstein E. S., 2015, *ApJ*, **801**, 3  
 Mikkola S., Merritt D., 2008, *AJ*, **135**, 2398  
 Naoz S., Fabrycky D. C., 2014, *ApJ*, **793**, 137  
 Naoz S., Farr W. M., Rasio F. A., 2012, *ApJ*, **754**, L36  
 Naoz S., Farr W. M., Lithwick Y., Rasio F. A., Teyssandier J., 2013a, *MNRAS*, **431**, 2155  
 Naoz S., Kocsis B., Loeb A., Yunes N., 2013b, *ApJ*, **773**, 187  
 Ngo H., et al., 2015, *ApJ*, **800**, 138  
 Pelupessy F. I., van Elteren A., de Vries N., McMillan S. L. W., Drost N., Portegies Zwart S. F., 2013, *A&A*, **557**, A84  
 Petrovich C., 2015a, *ApJ*, **799**, 27  
 Petrovich C., 2015b, *ApJ*, **805**, 75  
 Petrovich C., Tremaine S., 2016, preprint, ([arXiv:1604.00010](https://arxiv.org/abs/1604.00010))  
 Portegies Zwart S., McMillan S. L. W., van Elteren E., Pelupessy F. I., de Vries N., 2013, *Computer Physics Communications*, **183**, 456  
 Rasio F. A., Ford E. B., 1996, *Science*, **274**, 954  
 Santerne A., et al., 2016, *A&A*, **587**, A64  
 Smirnov N., 1948, *Annals of Mathematical Statistics*, **19**, 279  
 Socrates A., Katz B., 2012, preprint, ([arXiv:1209.5723](https://arxiv.org/abs/1209.5723))  
 Socrates A., Katz B., Dong S., 2012, preprint, ([arXiv:1209.5724](https://arxiv.org/abs/1209.5724))  
 Storch N. I., Lai D., 2015, *MNRAS*, **448**, 1821  
 Storch N. I., Anderson K. R., Lai D., 2014, *Science*, **345**, 1317  
 Tanaka H., Takeuchi T., Ward W. R., 2002, *ApJ*, **565**, 1257  
 Udry S., Santos N. C., 2007, *ARA&A*, **45**, 397  
 Winn J. N., et al., 2011, *AJ*, **141**, 63  
 Wright J. T., Marcy G. W., Howard A. W., Johnson J. A., Morton T. D., Fischer D. A., 2012, *ApJ*, **753**, 160

Wu Y., Lithwick Y., 2011, [ApJ](#), **735**, 109  
Wu Y., Murray N., 2003, [ApJ](#), **589**, 605  
Zucker S., Mazeh T., 2002, [ApJ](#), **568**, L113